

Increased phase coherence length in a porous topological insulator

Alexander Nguyen ^{1,2,*}, Golrokh Akhgar,^{1,2,*†} David L. Cortie ^{2,3,4}, Abdulhakim Bake,³ Zeljko Pastuovic,⁴ Weiyao Zhao,^{1,2} Chang Liu,^{1,2} Yi-Hsun Chen,^{2,5} Kiyonori Suzuki ¹, Michael S. Fuhrer ^{2,5}, Dimitrie Culcer,^{2,6} Alexander R. Hamilton,^{2,6} Mark T. Edmonds ^{2,5} and Julie Karel^{1,2,†}

¹*Department of Materials Science and Engineering, Monash University, Clayton 3800, Victoria, Australia*

²*ARC Centre of Excellence in Future Low-Energy Electronics Technology, Monash University, Clayton 3800, Victoria, Australia*

³*Institute for Superconducting and Electronic Materials, University of Wollongong, North Wollongong 2522, New South Wales, Australia*

⁴*Australian Neutron Science and Technology Organisation, New Illawarra Road, Lucas Heights NSW 2234, New South Wales, Australia*

⁵*School of Physics and Astronomy, Monash University, Clayton 3800, Victoria, Australia*

⁶*School of Physics, The University of New South Wales, Sydney 2052, New South Wales, Australia*



(Received 13 December 2022; revised 27 March 2023; accepted 6 April 2023; published 15 June 2023)

The surface area of Bi_2Te_3 thin films was increased by introducing nanoscale porosity. Temperature dependent resistivity and magnetotransport measurements were conducted both on as-grown and porous samples (23 and 70 nm). The longitudinal resistivity of the porous samples became more metallic, indicating the increased surface area resulted in transport that was more surfacelike. Weak antilocalization was present in all samples, and remarkably the phase coherence length doubled in the porous samples. This increase is likely due to the large Fermi velocity of the Dirac surface states. Our results show that the introduction of nanoporosity does not destroy the topological surface states but rather enhances them, making these nanostructured materials promising for low energy electronics, spintronics and thermoelectrics.

DOI: [10.1103/PhysRevMaterials.7.064202](https://doi.org/10.1103/PhysRevMaterials.7.064202)

I. INTRODUCTION

Bi_2Te_3 is a three-dimensional (3D) topological insulator (TI) characterized by an insulating bulk and topological metallic surface states [1–4]. The electronic structure of the surface states exhibits a linear dispersion relation and spin-momentum locking. Additionally, the surface states are topologically protected from backscattering, and are therefore appealing for low energy electronics since dissipationless currents can be achieved [3,5–7]. Owing to the unique electronic properties and large spin-orbit coupling, 3D TIs also exhibit efficient charge to spin current conversion arising from the spin-momentum locking in the surface states [8,9]. The largest reported spin orbit torque [10] has been found using a 3D TI, making this class of materials particularly promising for future spintronic devices [11–13].

Magnetotransport experiments have been extensively utilized to probe the topological surface states. In TIs, these states exhibit weak antilocalization (WAL) in their magnetoconductivity due to spin-momentum locking. According to the theory, the charge carriers move in 2π circles above the Dirac point and the π -Berry phase associated with these helical surface states changes the interference of the incoming and outgoing time-reversal paths from constructive to destructive [14–16]. The quantum correction to the conductivity of the 2D systems with strong spin-orbit coupling was initially derived

by Hikami, Larkin, and Nagaoka (HLN) [17] and Bergmann described the intuitive picture of WAL [18,19]. In the case of surface states in TIs, the WAL correction is similar to the correction described by HLN as the two systems are expected to be in the same universality class of 2D systems. However, in contrast to other 2D systems, there is no crossover from WAL to weak localization (WL) in TIs with increasing magnetic fields as the spins in the Dirac surface states of the TI are perfectly locked to momentum [16]. Typically 2D magnetoconductivity can be described using the HLN formulation in order to extract information about the nature of the transport (e.g., phase coherence length, decoherence mechanisms, number of conducting channels, 2D versus 3D scattering, etc.) [17,18]. Studies have shown the characteristics of the quantum transport can be controlled through, for instance, gating, doping, film thickness, a capping layer, or surface impurities [20–26]. Despite the fact that the phenomena being probed are present on the surface, the vast majority of these studies were conducted with a constant surface to volume ratio.

A conventional path to increase the surface to volume ratio is through the introduction of porosity [27]. This will typically also increase the disorder in the material; therefore, most work has avoided porous materials. Research has traditionally been directed towards studying highly ordered crystals with very low defect densities and impurity concentrations [21,28–30]. However, recent theoretical work has predicted the existence of topological conductive surface states and insulating bulk states in amorphous materials [31–33]. These theoretical models concluded that in the bulk of the material there are energies that are not eigenvalues of the Hamiltonian, i.e., there is a bandgap in the bulk. By contrast, on the surface where

*These authors contributed equally to this work

†Corresponding authors: gol.akhgar@monash.edu; julie.karel@monash.edu

the amorphous solid interfaces with a vacuum, these energy values become eigenvalues of the Hamiltonian. The study conducted by Costa *et al.* in particular is notable for modeling the density of states in amorphous bismuthene instead of a generic amorphous material [33]. Moreover, an exciting recent study has found that a topological phase transition from trivial insulator to TI can be induced by making a topologically trivial crystalline material either disordered [34] or amorphous [35]. These theoretical studies point to exciting possibilities to discover topological properties in disordered materials, a prospect which has been largely unexplored experimentally.

In this work, we introduce nanoscale porosity in Bi_2Te_3 in order to modify the surface to volume ratio. We will show that increasing the surface area, while also increasing disorder, leads to an enhancement in the WAL effect and, remarkably, a doubling of the phase coherence length. We suggest that the larger phase coherence length in the porous samples arises from an increased fraction of surface states, which have a higher velocity, contributing to the magnetoresistance.

II. EXPERIMENTAL METHODS

Nanocrystalline Bi_2Te_3 thin films were grown at room temperature on amorphous SiN_x on Si substrates using molecular beam epitaxy in an ultrahigh vacuum environment with a base pressure as low as 10^{-10} mbar. For Bi_2Te_3 film growth, effusion cells were used to evaporate elemental Bi (99.999%) and Te (99.95%) while the sample's temperature was kept at room temperature. Rates were calibrated with a quartz crystal microbalance before the growth. The Bi_2Te_3 thin films were grown using a 2:3 ratio of flux rates of Bi and Te. The films studied in this work were 23- and 70-nm thick.

To enable transport measurements, the films were grown through a shadow mask in the shape of a Hall bar with a channel length and width of 1 mm and 0.2 mm, respectively [Fig. 1(a)]. Ion irradiation was carried out using a 40 keV beam of Ne ions. The flux of ions irradiated on the sample was set to 1×10^{16} ions per cm^2 . Films were characterized before and after irradiation using JEOL JEM 2010 high resolution transmission electron microscopy (HRTEM) and a JEM-F200 multipurpose electron microscope. Raman and energy-dispersive x-ray spectroscopy (EDS) was also conducted to examine the structure and composition of the cross section. Temperature (2–300 K) and magnetic field-dependent (± 2 T) longitudinal resistivity and temperature-dependent Hall effect measurements were performed in a Quantum Design Physical Properties Measurement System. Both AC and DC measurements were performed in constant current mode with an applied current of 350–400 nA and 3–5 μA , respectively. The AC measurements used a lock-in technique at 17 Hz. The same results were obtained from AC and DC measurements, as verified by measurements conducted on the same sample using the two techniques.

III. RESULTS AND DISCUSSION

Nanocrystalline Bi_2Te_3 thin films were grown through a shadow mask using molecular beam epitaxy [Fig. 1(a)]. HRTEM measurements on the as-grown films indicated a

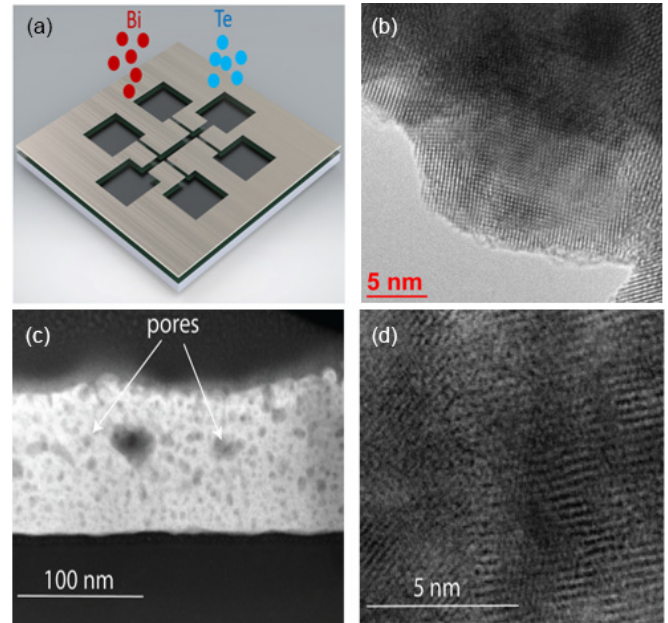


FIG. 1. (a) Bi_2Te_3 growth through a shadow mask with Hall bar geometry onto a SiN_x substrate with a channel length and width of 1 mm and 0.2 mm, respectively. (b) High angle annular dark field (HAADF) TEM image of as-grown Bi_2Te_3 . Image was taken using a FEI Tecnai G2 T20 TWIN TEM. (c) Low magnification HAADF cross-sectional TEM image of the 70 nm thick irradiated Bi_2Te_3 Hall bar. The cross-section was prepared after transport measurements were conducted. The irradiated Ne ions produced pores (dark) dispersed throughout the Bi_2Te_3 thin film (light). (d) High magnification bright field image of the same sample depicting the nanocrystalline structure.

nanocrystalline structure, with an average crystal size of ~ 20 nm. Figure 1(b) is the high angle annular dark field (HAADF) TEM image of as-grown Bi_2Te_3 taken using a FEI Tecnai G2 T20 TWIN TEM. Figure 1(c) displays HAADF cross-sectional TEM of the ion-irradiated 70-nm thin film. Nanoscale porosity can be observed throughout the entire film; the majority of the pores (99%) are between 1 and 10 nm in size. Upon examination of a 2D cross sectional TEM image, approximately 22% of the area contained voids (see Supplemental Material [36]). Figure 1(d) depicts a bright field image of the same sample at higher magnification. The energy-dispersive x-ray spectroscopy (EDS) measurement confirms that Ne ions were able to penetrate the entire thickness of the thin film which created porosity and left cavities throughout the whole material. EDS measurements show that no Ne ions were detected after ion irradiation and the sample is slightly Te poor (see Supplemental Material [36]).

Figures 2(a) and 2(b) show the normalized magnetoresistance ($(\rho_{xx}(B) - \rho_{xx}(0))/\rho_{xx}(B=0)$) as a function of applied magnetic field for the 23 nm as-grown and porous samples at various temperatures (see Supplemental Material for 70-nm samples [36]). These curves are representative of all samples measured and show positive magnetoresistance due to WAL. In TIs, this quantum coherent transport arises due to spin momentum locking of the topological surface states [14–16]. The WAL correction occurs at sufficiently low temperatures,

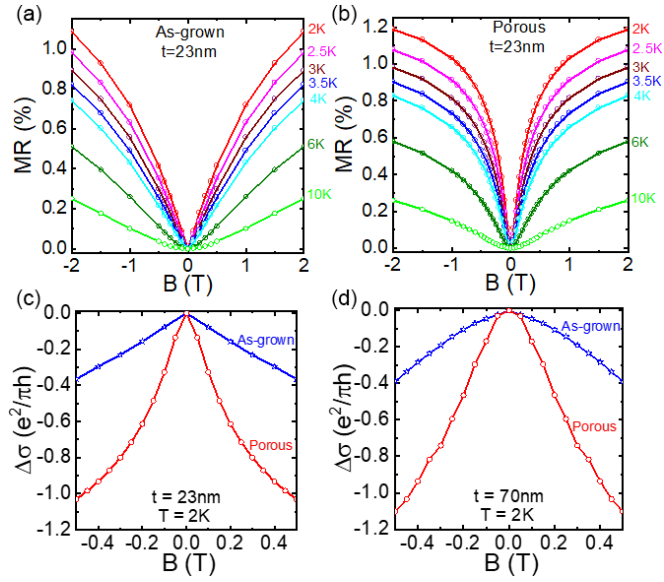


FIG. 2. (a) and (b) Normalized magnetoresistance % ($MR = (\rho_{xx}(B) - \rho_{xx}(0)) \times 100 / \rho_{xx}(B = 0)$) as a function of magnetic field for the 23 nm as grown and porous Bi_2Te_3 , respectively, at different temperatures.

and in these samples is not present above ~ 12 K, at which point the magnetoresistance is parabolic. Figures 2(c) and 2(b) compares the magnetoresistance at 2 K for the porous and as-grown samples of different thicknesses. The WAL effect is more pronounced at 2 K in the porous sample compared to the as-grown sample for both sample thicknesses. Remarkably, Figs. 2(c) and 2(d) show that the introduction of porosity has a significant effect on the magnetotransport and actually strengthens the WAL effect. The low field cusp is much stronger in the porous samples for both thicknesses, and this observation is true for all temperatures up to 10 K (see Supplemental Material [36]). The WAL interference effect is reduced with increasing magnetic field as a result of the additional phase introduced by the applied field. Therefore, in order to analyze the 2D WAL data accurately, the quantum transport correction should be limited to low fields ($B < 0.5$ T), and the HLN 2D localization theory is derived for the transport correction in low magnetic field only [17,18].

To probe the origins of the quantum transport, the 2D magnetoconductivity data has been fit using the reduced HLN formula [17,18]:

$$\Delta\sigma_{xx} = -\frac{\alpha e^2}{\pi h} \left[\ln\left(\frac{\hbar}{4eBL_\phi^2}\right) - \Psi\left(\frac{1}{2} + \frac{\hbar}{4eBL_\phi^2}\right) \right], \quad (1)$$

where B is the applied magnetic field perpendicular to the sample, Ψ is the digamma function, e is an elementary charge, L_ϕ is the phase coherence length and α is a coefficient relating to the conduction channels [17]. Figures 3(a) and 3(b) shows a representative fit for the porous 23 and 70 nm film up to 0.5 T (see Supplemental Material for other samples [36]). The prefactor α provides information about the channels contributing to the conduction; each conducting channel contributes -0.5 . WAL is a competition between phase decoherence and surface to bulk scattering. If the phase coherence time is much

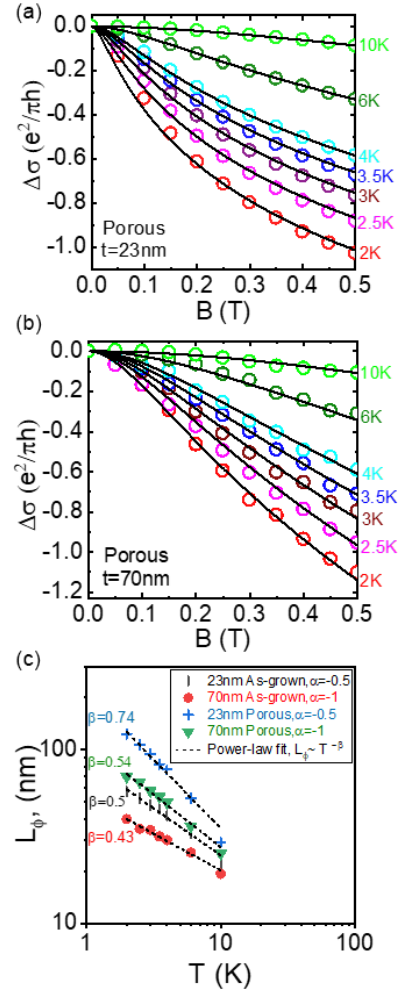


FIG. 3. (a) 2D magnetoconductivity of porous Bi_2Te_3 with thickness of 23 nm and (b) 70 nm at various temperatures. The solid black line is the fit to the reduced HLN formula. (c) The temperature dependence of the phase coherence length of 23 nm as-grown (black vertical lines), 70 nm as-grown (red circles), 23 nm porous (blue crosses) and 70 nm porous (green triangles) Bi_2Te_3 samples in log-log scale. The dashed line is the fit to the power law, $L_\phi \sim T^{-\beta}$.

larger than the surface to bulk scattering time, substantial surface-bulk scattering will occur and the sample will have a single transport channel with $\alpha = -0.5$. On the other hand, if the surface to bulk scattering time is large in comparison to the phase decoherence time, the top and bottom surfaces will be decoupled and each contribute -0.5 to the conduction, resulting in $\alpha = -1.0$ [20–22,25,26,37,38]. In the 23-nm samples, $\alpha = -0.5$, indicating the surface and bulk are coupled and behave as a single transport channel. By contrast, the 70-nm samples show $\alpha = -1.0$, meaning the top and bottom surfaces are decoupled; the increase in thickness likely results in a more significant effect of the bulk conductivity which reduces the coupling between the surfaces.

Some studies on topological materials have found a thickness dependence of α where α is approximately -0.5 in the thinnest samples and approaches -1 in the thicker samples. A recent study by Kumar *et al.* have found that when the temperature is less than or equal to 2 K samples as thin as

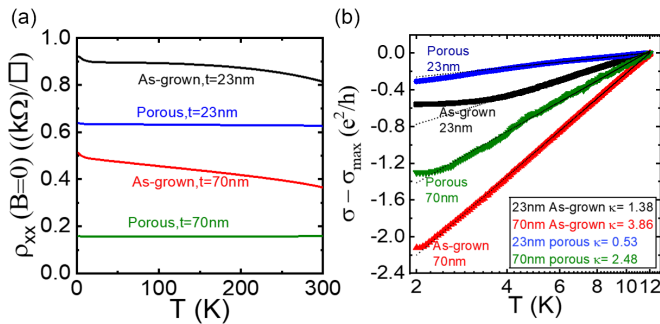


FIG. 4. (a) Temperature dependence of 2D sheet resistivity and (b) logarithmic temperature-dependent conductivity at zero magnetic field for as-grown 23nm (black line), as-grown 70 nm (red line), porous 23 nm (blue line) and porous 70 nm (green line) samples. The black dashed lines in (b) are the linear fit to the data.

5 nm exhibits an α of ≈ -0.5 but as the sample gets thicker (as thick as 20 nm) α approaches -1 [39]. Each transport channel has a -0.5 contribution to α ; the authors suggest that surface transport dominates the thinner samples whereas the thicker ones have the surface and the bulk acting as 2 different channels. Similarly, experiments done by Gautam *et al.* found that a 40 nm thick film of Bi_2Se_3 exhibited an α value of -0.65 , meanwhile, a film 80-nm thick displayed an α value of -0.83 [40]. The authors explain these values by stating that “the increasing value of α with increasing film thickness describes the contribution of surface states to the conduction is weak for [the] thicker film.” Finally, a study by Zhang *et al.* on 30 nm of Bi_2Se_3 determined that α was -0.34 ; as thickness increased α gradually decreased to a value of -0.72 in a 300-nm-thick sample [41]. Zhang *et al.* argue “that the top surface is only partially decoupled” hence α is between -0.5 and -1 . It is apparent from these studies that in our experiment the thinnest as-grown and porous Bi_2Te_3 samples have their top and bottom surfaces coupled into a single transport channel. As the samples get thicker a second transport channel develops. It is difficult to discern, however, whether the second transport channel is due to the bulk or due to the two surfaces becoming decoupled.

Figure 3(c) shows the temperature dependence of the phase coherence length (L_ϕ) extracted from the reduced HLN fits. Depending on the dimensionality of the system, L_ϕ follows a power law scaling $L_\phi \propto T^{-\beta}$ with $\beta = 0.5$ for 2D Nyquist dephasing and 0.75 for 3D Nyquist dephasing [42–46]. Surprisingly, for both sample thicknesses the phase coherence length approximately doubles with the introduction of porosity.

Figure 4(a) shows the longitudinal 2D resistivity (ρ_{xx}) as a function of temperature for the 23- and 70-nm as-grown and porous films. After ion irradiation, ρ_{xx} for a given thickness surprisingly decreases, indicating the samples become more metallic. The charge carrier densities for these samples, as determined by Hall effect measurements, ranged from 4.8×10^{20} to $1.5 \times 10^{21} \text{ cm}^{-3}$; all samples except the 70-nm porous sample were n type. (See Supplemental Material [36].) Given the porous samples are Te poor, p -type behavior would be expected for the 23-nm porous sample as well. The relatively high carrier densities and the unexpected sign of the

carriers is likely due to charge puddling; a further analysis of the MR behavior confirmed this result (see Supplemental Material for details [36]).

The as-grown samples exhibit a low temperature ($T < 12$ K) upturn that is attributed to the logarithmic quantum interference corrections to the Drude conductivity $\Delta\sigma \approx \ln T$ that are characteristic in 2D systems [e.g., WL, WAL and electron-electron interaction (EEI)] [44,45,47–52]. The resistivity is expected to decrease in the presence of WAL; therefore the observed increase in the resistivity with decreasing temperature in Fig. 4(a) can only be associated with WL or EEI. Furthermore, in the case of TIs in the absence of backscattering, quantum interference effects lead only to WAL and EEI in systems with strong spin-orbit interactions [16,20]. Therefore, this upturn in resistivity at reduced temperature ($T < 12$ K) in Fig. 4(a) is likely due to EEI effects. Figure 4(b) illustrates the logarithmic temperature-dependent conductivity $\sigma(T)$ curves for all four samples. All curves are normalized by their maximum conductivities (e.g., the conductivity at 12 K). The linear slope of these curves are extracted and can be defined as $\kappa = (\pi h/e^2) (\partial\sigma/\partial \ln T)$ which is given in the legend of Fig. 4(b). A steeper slope indicates a larger κ which means greater EEI [43,48,53]. The thicker samples (70 nm) show a higher κ compared to the thinner samples (23 nm) which indicates a stronger EEI correction to the Drude conductivity at low temperature. A similar thickness dependence effect has been observed recently in polycrystalline Bi_2Se_3 [38].

EEI and WAL are competing effects; at low temperatures, EEI will result in a decrease in conductivity whereas WAL produces a conductivity increase. So, it follows that the porous samples with an enhanced WAL exhibit a reduction in the EEI correction compared to the as-grown samples. The EEI reduction here [κ reduction in Fig. 4(b)] is comparable to an experimental study where the EEI is reduced after fabricating nanostructured Bi_2Te_3 thin films [54].

The most surprising result of this study is the fact that the phase coherence length doubled in the porous samples. Porosity increases the surface to bulk ratio, meaning the surface states contribute a larger fraction to the overall magnetotransport. The fact that the longitudinal resistivity decreases (compared to the as-grown) and is metallic in the porous samples indicates that the transport is primarily surfacelike. Given the linear dispersion of Dirac states on the surface, the Fermi velocity (v_F) is expected to be large in comparison to the bulk since it is proportional to the slope of energy (E) versus \mathbf{k} in momentum space [55]. It is important to note that the phase coherence length is proportional to v_F , that is $L_\phi = \sqrt{D\tau_\phi}$ and $D = v_F^2 \tau/d$, where τ_ϕ is the electron dephasing time, D is the electron diffusion constant, τ is the electron elastic mean free time and d is the system dimension [56]. Therefore, the large v_F of the surface states could result in the enhanced L_ϕ observed in the porous samples.

Our results indicate that the introduction of porosity produces disorder but does not destroy the topological surface states in the material. On the contrary, the phase coherence length nearly doubled. Such a result is promising for practical integration of topological insulators into future low energy electronic and spintronic devices, where disorder can be very difficult to eliminate entirely. Moreover, work has predicted

that the porosity in a topological insulator can produce a large thermoelectric figure of merit due to the high contribution of the metallic surface states and suppressed phonon thermal conductivity [27]. Our work has experimentally shown that it is indeed possible to introduce porosity while still maintaining the metallic surface states, pointing to the promise of porous TIs in thermoelectric devices.

IV. CONCLUSIONS

Temperature dependent resistivity and magnetotransport measurements were conducted on as-grown and porous Bi₂Te₃ thin films. Ion irradiation was used to introduce nanoscale porosity in the material, which increased the surface to volume ratio. The temperature dependence of the longitudinal resistivity indicates the porous films exhibit metalliclike behavior owing to the increased surface state contribution. The EEI correction to the conductivity is present in all samples but stronger in the as-grown films. In contrast, the porous TIs exhibit stronger WAL and surprisingly a longer phase coherence length compared to the as-grown film. The larger phase

coherence length is attributed to the large v_F of the Dirac surface states. This work suggests porosity is an effective means to enhance the topological surface states' contribution to the transport, making these materials promising for low energy electronics, spintronics and thermoelectrics.

ACKNOWLEDGMENTS

A.N., G.A., J.K., M.T.E., D.L.C., D.C., A.R.H., and M.S.F. acknowledge the funding support from the Australian Research Council Centre of Excellence in Future Low Energy Electronics Technologies (CE170100039). J.K. acknowledges the support from the Australian Research Council Discovery Projects (DP200102477 and DP220103783). This work was performed in part at the Melbourne Centre for Nanofabrication (MCN) in the Victorian Node of the Australian National Fabrication Facility (ANFF). The ion irradiation of this research was undertaken in Australian Neutron Science and Technology Organisation (ANSTO). We would like to acknowledge Professor S. Praver and use of his laser cutter facility at the University of Melbourne in making the shadow masks.

-
- [1] L. Fu, C. L. Kane, and E. J. Mele, *Phys. Rev. Lett.* **98**, 106803 (2007).
- [2] Y. L. Chen, J. G. Analytis, J.-H. Chu, Z. K. Liu, S.-K. Mo, X.-L. Qi, H. J. Zhang, D. H. Lu, X. Dai, and Z. Fang, *Science* **325**, 178 (2009).
- [3] H. Zhang, C.-X. Liu, X.-L. Qi, X. Dai, Z. Fang, and S.-C. Zhang, *Nat. Phys.* **5**, 438 (2009).
- [4] M. Zahid Hasan and J. E. Moore, *Annu. Rev. Condens. Matter Phys.* **2**, 55 (2011).
- [5] D. Hsieh, Y. Xia, D. Qian, L. Wray, F. Meier, J. H. Dil, J. Osterwalder, L. Patthey, A. V. Fedorov, H. Lin *et al.*, *Phys. Rev. Lett.* **103**, 146401 (2009).
- [6] D. Hsieh, Y. Xia, D. Qian, L. Wray, F. Meier, J. Osterwalder, L. Patthey, J. G. Checkelsky, N. P. Ong, and A. V. Fedorov, *Nature (London)* **460**, 1101 (2009).
- [7] M. Z. Hasan and C. L. Kane, *Rev. Mod. Phys.* **82**, 3045 (2010).
- [8] C. H. Li, O. M. J. Van't Erve, J. T. Robinson, Y. Liu, L. Li, and B. T. Jonker, *Nat. Nanotechnol.* **9**, 218 (2014).
- [9] A. Dankert, P. Bhaskar, D. Khokhriakov, I. H. Rodrigues, B. Karpiak, M. Venkata Kamalakar, S. Charpentier, I. Garate, S. P. Dash, and P. Saroj, *Phys. Rev. B* **97**, 125414 (2018).
- [10] M. Dc, R. Grassi, J.-Y. Chen, M. Jamali, D. R. Hickey, D. Zhang, Z. Zhao, H. Li, P. Quarterman, and Y. Lv, *Nat. Mater.* **17**, 800 (2018).
- [11] I. Žutić, J. Fabian, and S. D. Sarma, *Rev. Mod. Phys.* **76**, 323 (2004).
- [12] N. Huynh Duy Khang, Y. Ueda, and P. N. Hai, *Nat. Mater.* **17**, 808 (2018).
- [13] N. Huynh Duy Khang, S. Nakano, T. Shirokura, Y. Miyamoto, and P. N. Hai, *Sci. Rep.* **10**, 12185 (2020).
- [14] M. V. Berry, *Proc. R. Soc. London Ser. A* **392**, 45 (1984).
- [15] L. Fu and C. L. Kane, *Phys. Rev. B* **76**, 045302 (2007).
- [16] D. Culcer, *Physica E* **44**, 860 (2012).
- [17] S. Hikami, A. I. Larkin, and Y. Nagaoka, *Prog. Theor. Phys.* **63**, 707 (1980).
- [18] G. Bergmann, *Solid State Commun.* **42**, 815 (1982).
- [19] G. Bergmann, *Phys. Rev. B* **28**, 2914 (1983).
- [20] J. Chen, H. J. Qin, F. Yang, J. Liu, T. Guan, F. M. Qu, G. H. Zhang, J. R. Shi, X. C. Xie, C. L. Yang *et al.*, *Phys. Rev. Lett.* **105**, 176602 (2010).
- [21] H.-T. He, G. Wang, T. Zhang, I.-K. Sou, G. K. L. Wong, J.-N. Wang, H.-Z. Lu, S.-Q. Shen, and F.-C. Zhang, *Phys. Rev. Lett.* **106**, 166805 (2011).
- [22] Y. S. Kim, M. Brahlek, N. Bansal, E. Edrey, G. A. Kapilevich, K. Iida, M. Tanimura, Y. Horibe, S.-W. Cheong, and S. Oh, *Phys. Rev. B* **84**, 073109 (2011).
- [23] N. Bansal, Y. S. Kim, M. Brahlek, E. Edrey, and S. Oh, *Phys. Rev. Lett.* **109**, 116804 (2012).
- [24] D. Kim, S. Cho, N. P. Butch, P. Syers, K. Kirshenbaum, S. Adam, J. Paglione, and M. S. Fuhrer, *Nat. Phys.* **8**, 459 (2012).
- [25] P. H. Le, P.-T. Liu, C. W. Luo, J.-Y. Lin, and K. H. Wu, *J. Alloys Compd.* **692**, 972 (2017).
- [26] R. K. Gopal, S. Singh, A. Mandal, J. Sarkar, and C. Mitra, *Sci. Rep.* **7**, 1 (2017).
- [27] O. A. Tretiakov, A. Abanov, and J. Sinova, *Appl. Phys. Lett.* **99**, 113110 (2011).
- [28] D. Culcer, E. H. Hwang, T. D. Stanescu, and S. Das Sarma, *Phys. Rev. B* **82**, 155457 (2010).
- [29] P. Adroguer, W. E. Liu, D. Culcer, and E. M. Hankiewicz, *Phys. Rev. B* **92**, 241402(R) (2015).
- [30] W. E. Liu, E. M. Hankiewicz, and D. Culcer, *Materials* **10**, 807 (2017).
- [31] N. P. Mitchell, L. M. Nash, D. Hexner, A. M. Turner, and W. Irvine, *Nat. Phys.* **14**, 380 (2018).
- [32] A. Agarwala, in *Excursions in Ill-Condensed Quantum Matter* (Springer, Berlin, 2019), p. 61.
- [33] M. Costa, G. R. Schleder, M. B. Nardelli, C. Lewenkopf, and A. Fazzio, *Nano Lett.* **19**, 8941 (2019).
- [34] P. Corbae, F. Hellman, and S. M. Griffin, *Phys. Rev. B* **103**, 214203 (2021).

- [35] C. Wang, T. Cheng, Z. Liu, F. Liu, and H. Huang, *Phys. Rev. Lett.* **128**, 056401 (2022).
- [36] See Supplemental Material at <http://link.aps.org/supplemental/10.1103/PhysRevMaterials.7.064202> for information and additional figures on HRTEM, Raman, EEI, Hall Effect, charge puddling, magnetoresistance and fitting the magnetoconductivity data to HLN formula.
- [37] W. J. Wang, K. Hong Gao, and Z. Q. Li, *Sci. Rep.* **6**, 25291 (2016).
- [38] E. I. Rogacheva, O. Pavlosiuk, A. V. Meriuts, T. N. Shelest, A. Yu Sipatov, O. N. Nashchekina, K. V. Novak, and D. Kaczorowski, *Thin. Solid. Films* **743**, 139070 (2022).
- [39] Y. Kumar, P. Sharma, and V. P. S. Awana, *J. Mater. Sci.: Mater. Electron.* **33**, 18726 (2022).
- [40] S. Gautam, V. Aggarwal, B. Singh, V. P. S. Awana, R. Ganesan, and S. S. Kushvaha, *Sci. Rep.* **12**, 9770 (2022).
- [41] G. Akhgar, D. L. Creedon, L. H. W. Beveren, A. Stacey, D. I. Hoxley, J. C. McCallum, L. Ley, A. R. Hamilton, and C. I. Pakes, *Appl. Phys. Lett.* **112**, 042102 (2018).
- [42] A. Schmid, *Z. Phys.* **271**, 251 (1974).
- [43] B. L. Altshuler and A. G. Aronov, *Zh. Eksp. Teor. Fiz.* **77**, 2028 (1979).
- [44] B. L. Altshuler, A. G. Aronov, and D. E. Khmel'nitsky, *J. Phys. C* **15**, 7367 (1982).
- [45] P. A. Lee and T. V. Ramakrishnan, *Rev. Mod. Phys.* **57**, 287 (1985).
- [46] M. E. Gershenson, *Ann. Phys.* **511**, 559 (1999).
- [47] G. M. Minkov, O. E. Rut, A. V. Germanenko, A. A. Sherstobitov, V. I. Shashkin, O. I. Khrykin, and V. M. Daniltsev, *Phys. Rev. B* **64**, 235327 (2001).
- [48] K. E. J. Goh, M. Y. Simmons, and A. R. Hamilton, *Phys. Rev. B* **77**, 235410 (2008).
- [49] J. Wang, A. M. DaSilva, C.-Z. Chang, K. He, J. K. Jain, N. Samarth, X.-C. Ma, Q.-K. Xue, and M. H. W. Chan, *Phys. Rev. B* **83**, 245438 (2011).
- [50] A. L. Efros and M. Pollak, *Electron-Electron Interactions in Disordered Systems* (Elsevier, Amsterdam, 2012).
- [51] G. Akhgar, O. Klochan, L. H. W. Beveren, M. T. Edmonds, F. Maier, B. J. Spencer, J. C. McCallum, L. Ley, A. R. Hamilton, and C. I. Pakes, *Nano Lett.* **16**, 3768 (2016).
- [52] Y. Jing, S. Huang, K. Zhang, J. Wu, Y. Guo, H. Peng, Z. Liu, and H. Q. Xu, *Nanoscale* **8**, 1879 (2016).
- [53] B. L. Altshuler and A. Gh Aronov, in *Modern Problems in Condensed Matter Sciences* (Elsevier, Amsterdam, 1985), Vol. 10, p. 1.
- [54] H.-C. Liu, H.-Z. Lu, H.-T. He, B. Li, S.-G. Liu, Q. Lin He, G. Wang, I. K. Sou, S.-Q. Shen, and J. Wang, *ACS Nano* **8**, 9616 (2014).
- [55] F. Xiu, L. He, Y. Wang, L. Cheng, L.-T. Chang, M. Lang, G. Huang, X. Kou, Y. Zhou, and X. Jiang, *Nat. Nanotechnol.* **6**, 216 (2011).
- [56] J. J. Lin and J. P. Bird, *J. Phys.: Condens. Matter* **14**, R501 (2002).